ISSN 1028-334X, Doklady Earth Sciences, 2006, Vol. 407A, No. 3, pp. 401–407. © Pleiades Publishing, Inc., 2006.
Original Russian Text © S.G. Skolotnev, A.A. Peive, B.V. Belyatskii, 2006, published in Doklady Akademii Nauk, 2006, Vol. 407, No. 6, pp. 798–805.

GEOLOGY

Geochemical and Isotopic Features of Basalts in the Axial Mid-Atlantic Ridge near the Martin Vaz Fracture Zone, South Atlantic (19°–20° S)

S. G. Skolotnev, A. A. Peive, and B. V. Belyatskii

Presented by Academician Yu. M. Pushcharovsky October 11, 2005

Received October 12, 2005

DOI: 10.1134/S1028334X06030135

One of the essential problems of oceanic tectonics is estimation of the influence of plumes of the deep hot mantle on processes in the axial spreading zone. Areas of two giant (St. Helena and Tristan da Cunha) plumes in the Mid-Atlantic Ridge (MAR) rift zone (South Atlantic) are characterized by the effusion of basalts that differ from typical depleted riftogenic tholeiites by anomalously high contents of lithophile components and specific isotopic compositions [1]. Moreover, the rift valley floor with basalt effusion is significantly uplifted above the adjacent sectors of the rift.

The formation of the St. Helena Seamount located 400 km east of the MAR axis is related to magmatism that is active to this day [2]. St. Helena Island is a member of the structural ensemble of large volcanic seamounts (Bonaparte, Bagration, and Kutuzov) [3]. Like St. Helena Island, each seamount incorporates a series of smaller rises of different morphologies and dimensions. Thus, a system of subparallel series of NE-trending (~45°) rises extend from the seamount ensemble to the African continent. According to the plate tectonics concept, the seamount series represent hotspots related to a deep mantle plume that can be projected onto the present-day St. Helena Island area (St. Helena plume) [4]. At the same time, the inferred topographic map based on satellite altimetry data [5] (Fig. 1) shows that the seamount series also extend along the opposite southwestern direction (~225°) toward the axial MAR and even intersect the latter structure. This fact cannot be explained by the hotspot hypothesis, which suggests stationary positions of plumes relative to the mobile oceanic plate.

In the course of Cruise 10 of the R/V *Akademik Ioffe* (2002), detailed geological and geophysical investigations were carried out at the junction of one structural series with the MAR rift zone located near the Martin Vaz Fracture Zone (Martin Vaz test area, 19°–20° S) (Fig. 1). The present communication is devoted to the study of lithology, geochemistry, and isotopy of basalts dredged at the test area.

Results of a bathymetric survey at the Martin Vaz test area revealed a rift valley and surrounding rift-related seamount system of subparallel ridges [6]. At the junction of the axial MAR with one of the structural series extending from the seamount ensemble, the western wall of the rift valley incorporates a small oval seamount with the summit complicated by ridges striking parallel to the rift valley (Fig. 2).

Dredging in the course of Cruise 10 made it possible to sample the rift valley (stations I1048 and I1052), rift-related seamounts (stations I1047 and I1049), a seamount located at the bend of the rift valley (station I1051), and the oval seamount (station I1050) (Fig. 2). All of the samples structures are composed of basalts mainly represented by olivine–plagioclase–porphyry varieties on the seafloor and by aphyric varieties on the oval seamount slope.

The chemical composition of basalts was determined by conventional analytical methods in the chemical–analytical laboratory of the Geological Institute (Moscow). Trace elements in the samples were analyzed by the RFA method (Vernadsky Institute of Geochemistry and Analytical Chemistry, Moscow; E.P. Shevchenko, analyst). The results are presented in Table 1. In some representative samples, concentrations of rare earth and other minor elements were determined by the ICP-MS method (Vernadsky Institute of Geochemistry and Analytical Chemistry, Moscow; D.Z. Zhuravlev, analyst) (Table 2).

In terms of the composition and contents of trace elements, the basalts can be divided into two groups. Basalts of group 1 prevail along the rift segment (stations I1048, I1049, I1051, and I1052) and the second

Geological Institute, Russian Academy of Sciences, Pyzhevskii per. 7, Moscow, 119017 Russia; e-mail: skol@ginras.ru

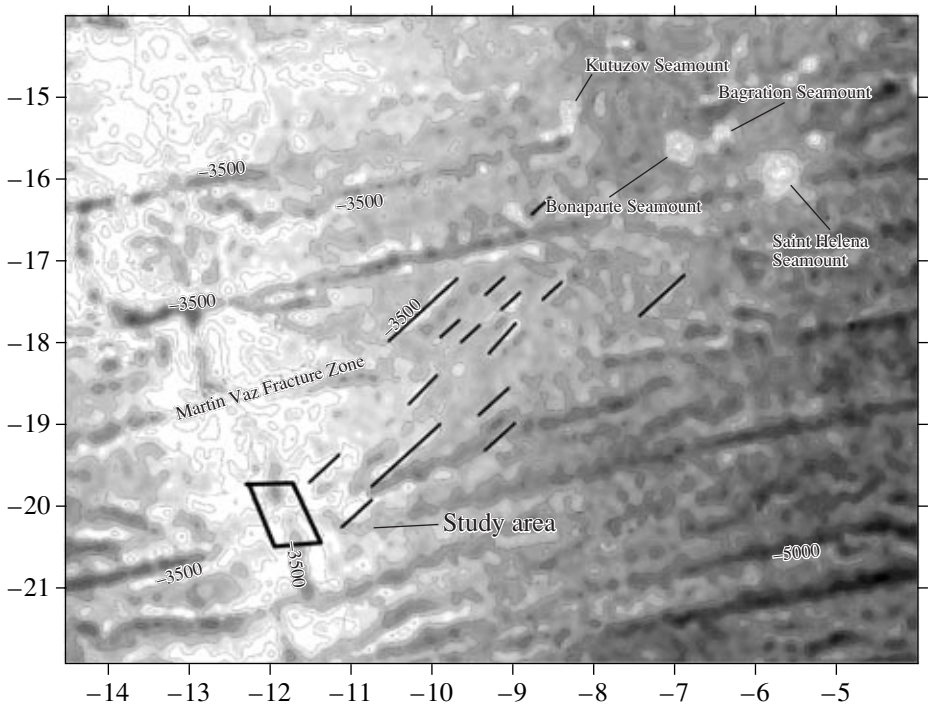

Fig. 1. Map of inferred topography of the study region and its vicinity. Compiled after data in [5]. The Martin Vaz test area is outlined. Black lines show axes of extended rises.

riftogenic seamount range on the western side (station I1047). Basalts of group 2 make up the oval seamount (station I1050).

Basalts of group 1 are characterized by an insignificant compositional variation primarily related to the degree of differentiation. For example, variation of the FeO*/MgO ratio, an indicator of the degree of differentiation, is insignificant within a single seamount. However, the FeO*/MgO ratio in basalts of one seamount differs from that of another seamount. In the north- to south-striking rift valley, variation in the FeO*/MgO ratio is as follows: 1.24–1.38 at station I1048, 1.09–1.14 at station I1052, 1.08–1.28 at I1051, and 1.41–1.64 at I1049. The older basalt from station I1047 has a higher FeO*/MgO value (1.53–1.69). This fact testifies to the nonstationary mode of processes in intermediate magma chambers both in space (in the case of recent processes) and in time. Table 1 shows that the coefficient of differentiation (FeO*/MgO) in the basalts has a positive correlation with TiO_2 (1.27–1.98%), Zr (78–130 ppm), V (260–360 ppm), K_2O (0.07–0.21%), P_2O_5 (0.09–0.16%), Y (28–41 ppm), and Ba (5–62 ppm). Correlation with Cr is negative (340–240 ppm). Variations in other elements do not depend on the FeO*/MgO ratio. Moreover, concentrations of lithophile elements in the basalts are very low (Nb 2–3.1 ppm, Sr 110–120 ppm). Sample I1049/21 is marked by higher concentrations of lithophile elements (K_2O 0.29%, Rb 3.3 ppm, and Nb 4.1 ppm). Basalts of this sample represent the weakly differentiated variety of a specific thermodynamic environment with high contents of TiO_2, Na_2O, P_2O_5, FeO*, Y, Zr, and Ni.

Relative to basalts of group 1, basalts of group 2 are characterized by significantly higher contents of lithophile elements (K_2O 0.35–0.46%, P_2O_5 0.20–0.21%, Ba 110–140 ppm, Rb 5.3–7 ppm, Nb 13 ppm, Sr 240–250 ppm, Ni 240–280 ppm, and Cr 490–540 ppm) and a lower degree of differentiation (FeO*/MgO = 0.77–0.95) (Table 1).

Basalts of groups 1 and 2 also differ in terms of contents of REEs and minor elements (Table 2). Basalts of group 1 with $(Nb/Zr)_n$ = 0.20–0.38 and $(La/Sm)_n$ = 0.56–0.64 can be referred to oceanic tholeiites of the N-MORB type that are products of the depleted mantle. Basalts of group 2 with $(Nb/Zr)_n$ = 1.36–1.43 and $(La/Sm)_n$ = 1.6 belong to tholeiites of the T-MORB type related to melting of the enriched mantle. In the REE distribution plot (Fig. 3), data points of group 1 are scattered along nearly horizontal lines typical of depleted tholeiites (slight rise in the HREE and MREE regions and significant fall in the LREE region). Basalts of group 2 are characterized by a steady rise in the curve from Lu to La and a constant slope.

The enriched basalt (sample I1050/10) is distinguished from other basalt samples by considerably higher Th concentrations (Table 2).

Among basalts of group 2, sample I1050/8 is marked by lower concentrations of LREE, Nb, Ni, and Cr (Tables 1, 2) and, correspondingly, lower values of $(Nb/Zr)_n$ and $(La/Sm)_n$ (0.77 and 1.06, respectively).

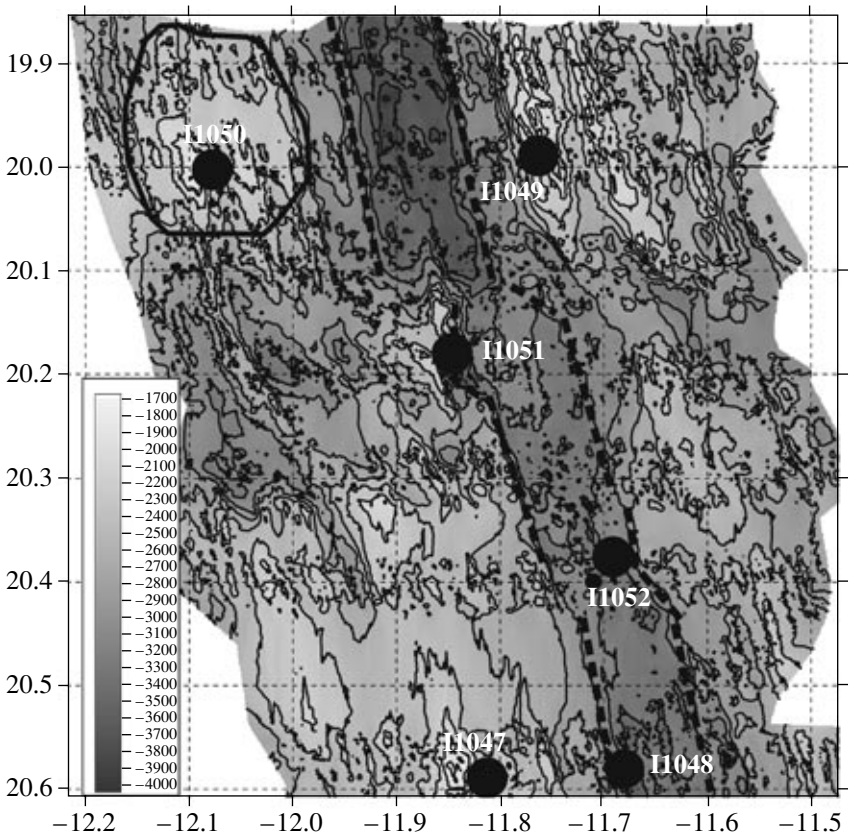

Fig. 2. Bathymetric chart of the Martin Vaz test area. Compiled after data in [6]. Circles show positions of dredging stations. Numerals designate the station number. Solid line outlines the oval rise; dotted lines, walls of the rift valley. The depth scale is given at the left lower corner. (St. I1047) 20°33.5′ W, 11°29.5′ S; depth 2500–2200 m; (St. I1048) 20°35.6′ W, 11°40.5′ S; depth 3600–3100 m; (St. I1049) 20°00.0′ W, 11°46.8′ S; depth 2800–2200 m; (St. I1050) 20°00.0′ W, 12°04.5′ S; depth 2400–2100 m; (St. I1051) 21°12.0′ W, 11°50.5′ S; depth 3500–3200 m; (St. I1052) 20°24.0′ W, 11°42.1′ S; depth 3200–3100 m.

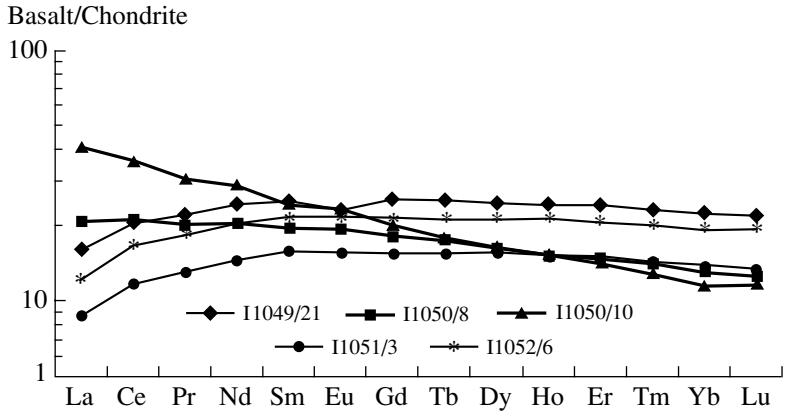

Fig. 3. REE distribution patterns in selected basalts.

Five samples of basalt 2 were examined for the isotopic composition of Pb, Sr, and Nd at the Institute of Precambrian Geology and Geochronology, St. Petersburg (Finnigan MAT 261 multichannel solid-phase mass spectrometer). Uncertainty of measurements was better than 0.005% (Sr and Nd) and 0.1% (Pb). The results are presented in Table 3 and Fig. 4 (based on isotope diagrams [7, 8]).

In the $^{206}Pb/^{204}Pb$–$^{208}Pb/^{204}Pb$ diagram, data points of the basalts are plotted nearly along the DMM–HIMU trend. Samples of group 1 are located in the depleted OIB field. Among samples of group 2, data point of sample I1050/8 (group 2) with the highest isotope ratio is sandwiched between the depleted OIB and Ascension Island fields, while data point of sample I1050/10 is slightly shifted toward higher $^{208}Pb/^{204}Pb$ values.

Table 1. Chemical composition and contents of trace elements in basalts (oxides are given in %; elements, in ppm)

Station	SiO_2	TiO_2	Al_2O_3	Fe_2O_3	FeO	MnO	MgO	CaO	Na_2O	K_2O	P_2O_5	L.O.I.	Total	Nb	Zr	Y	Rb	Sr	Ba	V	Ni	Cr	Co
Basalts of group 1																							
I1047/2	48.88	1.83	13.95	4.56	7.54	0.19	7.60	10.85	2.77	0.08	0.14	0.94	99.33	2.3	120	39	<1	110	45	340	92	260	52
I1047/3	48.64	1.98	12.82	6.55	6.75	0.19	7.60	10.19	2.95	0.21	0.16	1.49	99.53	2.4	130	41	3.5	110	45	350	130	240	60
I1047/5	49.02	1.94	13.16	6.03	7.36	0.19	7.55	10.14	2.90	0.18	0.16	0.98	99.61	2.3	120	39	1.6	110	62	360	98	240	57
I1048/1	49.24	1.61	14.00	4.40	7.40	0.18	8.24	10.86	2.89	0.14	0.12	0.82	99.90	2.2	105	34	1.5	120	50	320	130	350	49
I1048/3	49.32	1.49	15.42	3.31	6.65	0.17	7.76	11.09	2.89	0.17	0.11	0.94	99.32	1.9	96	31	1.2	130	29	300	110	310	51
I1049/1	48.32	1.58	15.67	5.63	5.86	0.17	6.67	11.20	2.73	0.20	0.12	1.21	99.36	2.6	100	34	2.7	110	29	300	110	245	46
I1049/14	47.98	1.50	16.65	4.19	6.29	0.16	7.11	11.31	2.60	0.14	0.11	1.28	99.32	2.8	100	30	1.5	110	23	280	110	220	41
I1049/16	47.84	1.53	16.95	4.59	5.82	0.15	7.07	10.98	2.65	0.20	0.11	1.40	99.29	2.6	95	31	2.4	110	10	300	110	240	46
I1049/21	48.66	1.98	14.48	7.38	4.79	0.19	7.40	10.17	2.90	0.29	0.17	1.01	99.42	4.1	120	39	3.3	115	30	410	94	250	62
I1049/30	49.26	1.95	15.40	5.40	5.72	0.19	7.51	10.59	2.90	0.23	0.17	0.46	99.78	3.1	125	41	1.7	120	46	380	140	250	59
I1051/3	48.99	1.27	18.20	3.72	4.54	0.15	7.29	12.16	2.60	0.18	0.09	0.47	99.66	2.2	78	28	2.7	120	5	280	97	290	45
I1051/5	48.43	1.31	17.02	5.16	4.69	0.16	7.52	11.68	2.62	0.17	0.09	0.84	99.69	2.3	81	27	2.4	120	5	260	100	310	49
I1051/8	49.46	1.41	15.59	3.88	5.62	0.16	8.05	12.17	2.88	0.07	0.10	0.72	100.11	2.5	88	28	<1	130	<5	300	92	340	46
I1051/9	49.83	1.47	15.98	2.04	7.42	0.17	7.21	12.31	2.90	0.14	0.11	0.77	100.35	3.1	90	28	8.3	130	<5	290	96	360	46
I1052/2	49.08	1.57	15.99	1.84	8.20	0.17	8.65	11.18	2.94	0.10	0.11	0.36	100.19	2.9	100	34	5.9	130	6	310	200	420	60
I1052/3	49.01	1.54	16.05	2.01	7.78	0.17	8.58	11.29	2.92	0.13	0.11	0.56	100.15	2.0	100	33	3.0	130	6	320	220	410	60
I1052/5	49.23	1.54	15.85	1.80	7.76	0.18	8.93	11.16	2.94	0.13	0.11	0.53	100.16	2.4	100	32	3.1	130	8	310	200	430	56
I1052/6	49.13	1.55	16.00	1.92	7.84	0.18	8.78	11.13	2.88	0.12	0.13	0.48	100.14	3.1	100	32	5.6	130	6	290	190	390	54
I1052/7	49.31	1.55	15.54	2.17	8.15	0.18	8.92	11.11	2.86	0.12	0.11	0.40	100.42	2.4	100	32	5.6	130	6	290	190	390	55
I1052/9	48.79	1.55	16.20	2.07	7.76	0.18	8.93	11.08	2.83	0.12	0.12	0.29	99.92	2.8	100	31	6.3	130	24	300	180	390	56
Basalts of group 2																							
I1050/5	47.83	1.69	14.55	4.54	5.68	0.17	10.27	10.67	2.63	0.35	0.21	1.26	99.85	13	100	23	5.3	240	140	270	270	540	60
I1050/6	47.79	1.61	14.51	4.54	4.15	0.14	10.73	10.12	2.64	0.28	0.20	2.82	99.53	13	105	22	3.7	250	110	250	280	530	57
I1050/8	49.47	1.61	16.02	4.95	4.20	0.15	7.74	11.16	2.64	0.42	0.15	1.03	99.54	6.9	98	27	7.0	180	110	280	130	290	48
I1050/10	47.98	1.66	14.96	3.52	6.19	0.16	10.22	10.36	2.64	0.46	0.21	1.31	99.67	13	105	25	6.6	240	110	260	240	490	55

Table 2. Contents of rare earth elements in selected basalts (ppm)

Station	La	Ce	Pr	Nd	Sm	Eu	Gd	Tb	Dy	Ho	Er	Tm	Yb	Lu	Hf	Ta	Pb	Th	U	$(La/Sm)_n$
I1049/21	3.80	12.37	2.09	11.25	3.84	1.34	5.17	0.94	6.21	1.36	3.97	0.58	3.78	0.55	3.36	0.26	0.61	0.18	0.14	0.64
I1050/8	4.89	12.89	1.90	9.44	2.97	1.12	3.71	0.65	4.11	0.86	2.44	0.35	2.21	0.32	2.40	0.50	0.51	0.40	0.20	1.06
I1050/10	9.70	22.00	2.89	13.46	3.70	1.34	4.11	0.67	4.18	0.87	2.32	0.33	1.95	0.29	2.54	0.96	1.09	1.07	0.32	1.69
I1051/3	2.07	7.16	1.24	6.76	2.41	0.91	3.17	0.58	3.95	0.86	2.45	0.36	2.36	0.34	2.00	0.10	0.36	0.07	0.08	0.55
I1052/6	2.86	10.14	1.74	9.48	3.30	1.26	4.41	0.79	5.36	1.19	3.41	0.51	3.24	0.49	2.49	0.11	0.76	0.09	0.04	0.56

Table 3. Sr–Nd–Pb isotope signatures of selected basalts

Station	$^{143}Nd/^{144}Nd$	$^{87}Sr/^{86}Sr$	$^{206}Pb/^{204}Pb$	$^{207}Pb/^{204}Pb$	$^{208}Pb/^{204}Pb$
I1049/21	0.512893	0.703027	18.384	15.483	37.903
I1050/8	0.513097	0.702967	19.022	15.534	38.395
I1050/10	0.512971	0.702604	18.155	15.579	38.075
I1051/3	0.513016	0.702502	18.046	15.548	37.874
Acidic leaching	0.513027	0.702457	18.093	15.521	37.912
I1052/6	0.512939	0.702912	18.412	15.467	38.149

In the $^{206}Pb/^{204}Pb$–$^{207}Pb/^{204}Pb$ plot, the majority of basalts are also arranged along the DMM–HIMU trend. Data points of basalt 1 fall into the depleted basalt field, whereas the data point of sample I1050/8 falls into the Iceland basalt field. However, data points of samples I1051/3 and I1050/10 with higher $^{207}Pb/^{204}Pb$ values are located approximately in the middle segment of the EM-1 and EM-2 join (Fig. 4).

Irrespective of group affiliation, the data points of all basalt samples are arranged along the DMM–HIMU trend in the $^{87}Sr/^{86}Sr$–$^{143}Nd/^{144}Nd$ plot; i.e., the basalts studied are similar to their counterparts in Ascension and St. Helena islands (Fig. 4).

Thus, the petrological and geochemical subdivision of basalts into two groups is partly supported by their isotopic signatures. The isotopic signature of basalt of group 1 is similar to that of the depleted OIB related to the melting of mantle substrate dominated by the DMM-type material.

The enriched basalt of group 2 (sample I1050/8) has higher $^{206}Pb/^{204}Pb$ and $^{208}Pb/^{204}Pb$ values, testifying to the possibility of generation of primary melt during the melting of depleted mantle contaminated with HIMU material. As was shown above, relative to other enriched basalts of group 2, this sample is characterized by lower concentrations of lithophile elements (in particular, Nb). This property is also typical of the HIMU source [7, 8]. Volcanics from St. Helena Island, products of the St. Helena plume, are the closest counterparts of the HIMU source. The isotopic–geochemical signature of the enriched basalt I1050/10 differs from that of sample I1050/8. The nature of its mantle substrate remains a debatable issue. The depleted mantle source in this case was evidently contaminated with a material enriched in lithophile elements and Th.

Geochemical and isotopic compositions of basalts from the studied MAR segment were investigated by Schilling [9] and Fontignie [1]. They only detected depleted basalts similar to basalts of group 1. Thus, we have discovered a new basalt-rich sector in the axial MAR in the North Atlantic. This basalt is related to the melting of a heterogeneous mantle substrate, the DM material of which can contain an admixture of the HIMU type or a component enriched in lithophile elements and Th. Basalts with similar geochemical signatures were previously reported from the northern South Atlantic. They were found in axial MAR segments (9°–11° S) and the St. Helena hotspot between the Ascension and St. Helena fracture zones (14°–17° S) [9]. In particular, data on the isotopic composition of basalts from these two anomalous MAE segments indicate that basalts of the MAR 14°–17° S segment were derived from a mantle substrate contaminated with material of the St. Helena plume [10]. Pb-, Sr-, and Nd-isotopic signatures of the enriched basalt I1050/8 (group 2) are similar to those of basalts from the MAR axial zone between 9°–11° S and 14°–17° S.

Taking into consideration the spatial association of anomalous basalts in the axial MAR and their isotopic–geochemical relationship with the adjacent hotspots, Schilling et al. [9] proposed that the St. Helena plume was intersected by a rift in the past. The subsequent westward migration of the rift produced an inclined conduit in the upper mantle. The plume material was transported via this conduit to the axial spreading zone and mixed with the DM material. This assumption is also supported by seismic tomography data [11]. They suggest that an inclined low-spreading zone splits off from the vertical low-spreading zone located beneath the St. Helena Rise and migrates toward the rift zone.

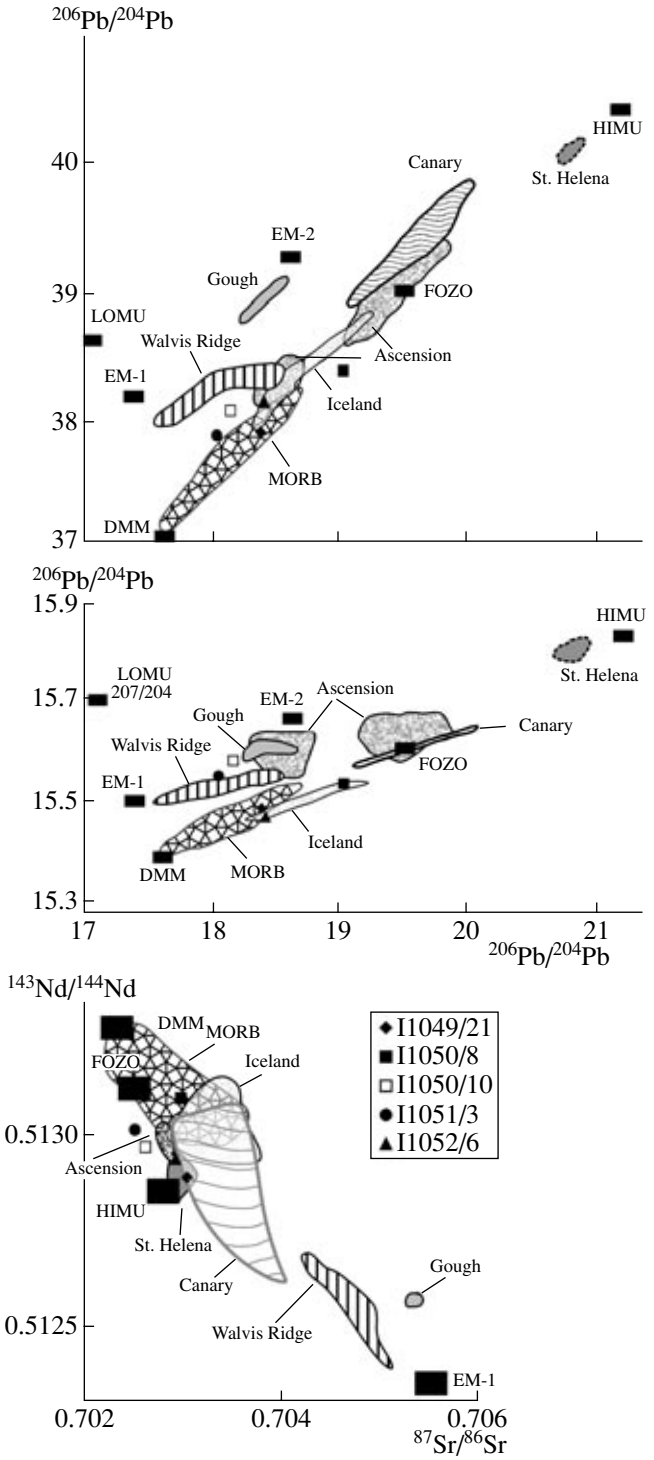

Fig. 4. Isotope diagrams. Compositional fields are given after [7, 8].

Based on the spatial proximity of the St. Helena plume and taking into consideration the isotopic–geochemical relationship of sample I1050/8 with volcanics from St. Helena Island, we suppose that material of the St. Helena plume was involved in the generation of basalt melts in the study area beneath the axial MAR. Furthermore, we can assume the following scenario for this process. As was mentioned above, zones between the axial MAR segment and the seamount ensemble (including St. Helena Island) are connected by a series of smaller seamounts (Fig. 1). The small oval seamount on the western wall of the rift valley probably represents a structural member of this series. Enriched basalts of group 2 are confined to the oval seamount. Therefore, we suppose that the St. Helena plume is separated from the rift valley located south of the Martin Vaz Fracture Zone by a permeable zone reaching the mantle zone. Material of the St. Helena plume could be injected into the permeable zone by the following two mechanisms:

(1) Lateral flow of material of the St. Helena plume not only along the direction nearly perpendicular to the spreading axis in line with the hypothesis suggested in [9], but also at some angle to the spreading axis along the direction opposite to that of lithospheric plates.

(2) Expansion of the St. Helena plume at the bottom, detachment of drops (microplumes) from the major plume body, and ascent of the microplumes along the inferred permeable zone.

The appearance of a higher-temperature plume material beneath the axial MAR could foster the melting of blocks of alien material enriched in lithophile elements and Th that were present in the asthenospheric diapir zone.

The permeable zone of the upper mantle level extended from the St. Helena Island region and adjacent seamounts to the MAR segment located near the Martin Vaz Fracture Zone. Intersection of one of the planetary-scale regmatic networks by the St. Helena plume could provoke the development of such a vast permeable zone. This assumption is supported by the existence of a series of young volcanic islands of the Cameroon line (Fernando Po, Principe, San Tome, and Annobon) [12] located near Africa. The volcanic islands are located at the northeastern flank of the seamount system mentioned at the beginning of the present communication. Materials discussed in the present communication show that enriched basalts near the Martin Vaz Fracture Zone have structural and isotopic–geochemical links with volcanics of St. Helena Island and Cameroon islands [13]. Therefore, one can suppose that all these structures make up a common (Cameroon) hot line in accordance with [14].

CONCLUSIONS

1. The axial MAR region near the Martin Vaz Fracture Zone (19°–20° S) in the South Atlantic incorporates a new depleted basalt segment with basalts enriched in lithophile elements. Isotope characteristics of the enriched basalts suggest their origination from a heterogeneous mantle substrate related to the mixing of DM material with the HIMU-type material.

2. The enriched basalts make up a small oval seamount on the western wall of the rift valley located on the SW-striking (225°) continuation of the seamount system extending from the St. Helena Seamount and adjacent large seamounts.

3. We believe that anomalous basalts appeared in the studied axial MAR zone as a result of spreading of mantle material of the St. Helena plume along a permeable zone extending along one of the diagonal fracture systems of the planetary regmatic network.

ACKNOWLEDGMENTS

This work was accomplished within the framework of the Program of Basic Research sponsored by the Presidium of the Russian Academy of Sciences ("Fundamental Problems of Oceanology: Geology, Geophysics, Biology, and Ecology"). It was supported by the Russian Foundation for Basic Research (project no. 03-05-64159) and the Federal Program "World Ocean" (Subprogram "Study of the Nature of the World Ocean").

REFERENCES

1. D. Fontignie and J. G. Schilling, Earth Planet. Sci. Lett. **142**, 109 (1996).
2. P. E. Baker, *The Ocean Basins and Margins. Vol. 1. The South Atlantic* (Elsevier, New York, 1973).
3. B. D. Uglov, Yu. G. Zorina, and M. K. Kaban, *The Angola–Brazil and Mascarene–Australia Geotraverses: Geological–Geophysical Atlas* (TsNIGRI, Moscow, 1999).
4. A. K. Martin, Tectonophysics, No. 142, 309 (1987).
5. D. T. Sandwell and W. H. F. Smith, J. Geophys. Res. **102** (B5), 10039 (1997).
6. S. G. Skolotnev, A. A. Peive, N. S. Bortnikov, et al., Dokl. Acad. Nauk **391**, 361 (2003) [Dokl. Earth Sci. **391**, 306 (2003)].
7. S. R. Hart, Earth Planet. Sci. Lett. **90**, 273 (1988).
8. A. F. Hofman, Nature **385** (6613), 219 (1997).
9. J. G. Schilling, G. Thompson, R. Kingsley, and S. Humphris, Nature **313** (5999), 187 (1985).
10. B. B. Hanan, R. Kingsley, and J. G. Schilling, Nature **322** (6080), 137 (1986).
11. Yu. Zhang, T. Tanimoto, and E. M. Stolper, Phys. Earth Planet. Inter. **84**, 79 (1994).
12. K. Burke, J. Geol. **109**, 349 (2001).
13. K. Rankenburg, J. C. Lassiter, and G. Brey, J. Petrol. **46**, 169 (2005).
14. A. A. Peive, *Lithostructural Inhomogeneities, Magmatism, and Geodynamic Features of the Atlantic Ocean* (Nauchnyi Mir, Moscow, 2002) [in Russian].